

## Dust in Supernovae; Formation and Evolution

Takashi Kozasa<sup>1</sup>, Takaya Nozawa<sup>2</sup>, Nozomu Tominaga<sup>3</sup>, Hideyuki Umeda<sup>4</sup>, Keiichi Maeda<sup>2</sup> & Ken'ichi Nomoto<sup>2,4</sup>

<sup>1</sup>*Department of CosmoSciences, Graduate School of Science, Hokkaido University, Sapporo 060-0810, Japan*

<sup>2</sup>*Institute for the Physics and Mathematics of the Universe, University of Tokyo, Kashiwa 277-8568, Japan*

<sup>3</sup>*Optical and Infrared Astronomy Division, National Astronomical Observatory of Japan, Mitaka 181-8588, Japan*

<sup>4</sup>*Department of Astronomy, School of Science, University of Tokyo, Tokyo 113-0033, Japan*

**Abstract.** Core-collapsed supernovae (CCSNe) have been considered to be one of sources of dust in the universe. What kind and how much mass of dust are formed in the ejecta and are injected into the interstellar medium (ISM) depend on the type of CCSNe, through the difference in the thickness (mass) of outer envelope. In this review, after summarizing the existing results of observations on dust formation in CCSNe, we investigate formation of dust in the ejecta and its evolution in the supernova remnants (SNRs) of Type II-P and Type IIb SNe. Then, the time evolution of thermal emission from dust in the SNR of Type IIb SN is demonstrated and compared with the observation of Cas A. We find that the total dust mass formed in the ejecta does not so much depend on the type;  $\sim 0.3 - 0.7M_{\odot}$  in Type II-P SNe and  $\sim 0.13M_{\odot}$  in Type IIb SN. However the size of dust sensitively depends on the type, being affected by the difference in the gas density in the ejecta: the dust mass is dominated by grains with radii larger than  $0.03 \mu\text{m}$  in Type II-P, and less than  $0.006 \mu\text{m}$  in Type IIb, which decides the fate of dust in the SNR. The surviving dust mass is  $\sim 0.04 - 0.2M_{\odot}$  in the SNRs of Type II-P SNe for the ambient hydrogen density of  $n_{\text{H}} = 10.0 - 1.0 \text{ cm}^{-3}$ , while almost all dust grains are destroyed in the SNR of Type IIb. The spectral energy distribution (SED) of thermal emission from dust in SNR well reflects the evolution of dust grains in SNR through erosion by sputtering and stochastic heating. The observed SED of Cas A SNR is reasonably reproduced by the model of dust formation and evolution for Type IIb SN.

### 1. Introduction

Dust is one of important ingredients in space to control the physical and chemical conditions in interstellar medium (ISM) and the formation process of stars in molecular clouds via the interactions with radiation and gas as well as the formation of  $\text{H}_2$  molecule on the surface. In astrophysical environments, dust grains form in a cooling gas outflowing from star to interstellar space such as in the stellar winds from asymptotic giant branch (AGB) stars and in the ejecta of novae and supernovae (SNe) where gas density is high enough to proceed the formation and growth of seed nuclei through collisions of relevant gas species.

Formation of dust in the ejecta of SNe had been invoked to explain the origin of interstellar dust (Cernuschi, Marsicano, & Codina 1967), and the microscopic analysis of individual grains in meteorites has identified the dust grains formed in SNe from their isotopic compositions (see Clayton & Nittler 2004 for a review). Dust formation in the ejecta of SNe had been directly observed for the first time in SN 1987A (see McCray 1993 for a review), after then dust formation in the ejecta was reported in a handful of core-collapsed SNe (CCSNe). Based on the observations of nearby SNe, the mass of dust formed in the ejecta has been considered to be less than  $10^{-3}M_{\odot}$  per SN, which is more than two to three orders of magnitude smaller than the dust mass predicted by theoretical investigations (Kozasa, Hasegawa, & Nomoto 1989, 1991; Todini & Ferrara 2001; Nozawa et al. 2003). Furthermore the observed dust mass is too small to explain the amount of dust observed in the host galaxies of quasars at redshift of  $z > 5$  (e.g. Bertoldi et al. 2003) where CCSNe are considered to be a major source of dust because the cosmic age is too young for AGB stars to supply the dust. So how much mass of dust forms in the ejecta has been still controversial.

In the ejecta of SNe, dust formation proceeds within the He-core where condensable elements are more abundant and the gas density is higher enough due to the smaller expansion velocity than in the outer envelope. How much mass and what kind of dust are injected from a SN into ISM depend not only on the formation in the ejecta but also on the destruction in the supernova remnant (SNR) where dust grains are injected into and eroded by sputtering in the hot gas swept up by the reverse and forward shocks produced by the interaction of ejecta with interstellar/circumstellar medium. Both processes depend on the type of SNe through the thickness (mass) of outer envelope: With the same kinetic energy of explosion, the thicker outer envelope makes the expansion velocity slower and results in the gas density within He-core being high enough to form large-sized dust. Furthermore, the lower gas density in the shocked region caused by the delayed arrival of the reverse shock at the dust forming region decreases the erosion rate of dust by sputtering.

In this review we show how the formation and destruction of dust in SNe depend on the type, comparing the results of calculations for Type II-P and Type IIb SNe; Type II-P SN is a typical type among CCSNe, and the well studied Cas A was recently identified as Type IIb SN (Krause et al. 2008). Then, we demonstrate the time evolution of thermal emission from dust residing in SNR of Type IIb SN, based on the results of calculations of dust formation and destruction. In § 2, we summarize the observations of dust formation in SNe after briefly introducing the classification of SNe. We present the results of calculations of dust formation in the ejecta of Type II-P and IIb SNe in § 3. Focusing on Type IIb SN, in § 4 we calculate the evolution of dust in the SNRs and the time evolution of thermal emission from dust, and compare with the observation of Cas A. Summary and concluding remarks are presented in § 5.

## 2. Observations of dust formation in supernovae

In this section we summarize the observations of dust formation in SNe. First we briefly introduce the classification of SNe for your information, and then review the observations of dust forming SNe. Massive stars whose main sequence mass

is larger than  $8 M_{\odot}$  end up their lives as CCSNe, but the details depend on the initial metallicity (Heger et al. 2003 for details). Here we shall confine to SNe evolved from stars with solar metallicity.

### 2.1. Classification of supernovae

Supernova is the most energetic explosion in the universe. Physically the supernovae are classified by the explosion mechanism; Core–collapsed supernovae which are triggered by the gravitational collapse of the central core, and thermonuclear supernovae in which the explosion energy is supplied by explosive thermonuclear burning (e.g. Hillebrandt & Niemeyer 2000).

Observationally SNe are classified by the spectral features at the early phase and the behavior of the light curve (e.g. Wheeler & Harkness 1990; Filippenko 1997; Leibundgut 2008). According to the presence of the H feature, SNe are divided into Type I and Type II; Type I without H, and Type II with H. Type I SNe are classified by the strength of the Si feature (Si II absorption at 6150 Å); Type Ia SNe showing the strong Si absorption feature are thermonuclear SNe whose progenitors are white dwarfs in binary systems. H–deficient Type I SNe with weak Si feature are subdivided by the content of He. He–rich is Type Ib and He–poor is Ic. The progenitors are Wolf–Rayet stars; H–envelope, and both H– and He–envelopes are removed before explosion for Type Ib SN and Type Ic SN, respectively, by stellar wind and/or interaction in binary system.

Type II SNe, whose progenitors are red supergiants, are divided by the content of H; H–poor are IIb SNe in which almost all of the H–envelope is removed during the evolution. H–rich Type II SNe are classified by the behavior of the light curves; the light curve linearly decays in Type II–L SNe, and have a plateau in Type II–P SNe. Type II SNe showing narrow emission lines originating in circumstellar medium are labelled as IIn. Type II, Ib and Ic SNe are core–collapsed supernovae.

### 2.2. Observations of dust formation in core–collapsed supernovae

Dust formation in the ejecta has been observed so far in the ejecta of CCSNe except for Type Ic SNe. No evidence of dust formation is reported in the ejecta of Type Ia SNe. Table 1 summarizes the observations of dust formation in the ejecta of CCSNe. Formation of dust in the ejecta had been confirmed observationally for the first time in SN 1987A which is a peculiar Type II SN because the progenitor is not a red supergiant but a blue supergiant (West et al. 1987).

The evidences of dust formation in the ejecta of SN 1987A (see McCray 1993; Wooden 1997; the references in Table 1) are the following; (1) the enhancement of infrared flux at  $\sim 10 \mu\text{m}$  starting from day 450 followed by the decline of U to M bolometric luminosity from  $\sim$  day 500, and (2) the appearance of blue–shifted profiles of [Mg I], [O I], [C I] lines starting from  $\sim$  day 530. The behavior of bolometric luminosity obtained by combining the observed U to M, infrared (thermal emission from dust), X-ray and  $\gamma$ –ray luminosities satisfies the energy budget expected from the decay of radioactive element  $^{56}\text{Co}$ . The appearance of blue–shifted lines was interpreted as the result of the attenuation of emission from the far (receding) side of the ejecta caused by dust grains formed in clumps within the ejecta, and in addition the intensities of [Mg I], [O I] and [Si I] lines concurrently decreased (Lucy et al. 1991). It should be noted

that, in prelude to the dust formation, formation of CO and SiO molecules was observed as early as day 112 and 165, respectively. The emission of SiO was no longer recognized at day 517 around which dust formation was confirmed by the observation of blue-shifted lines (Roche et al. 1991). The dust mass estimated from the observation was at least  $1 \times 10^{-4} M_{\odot}$  at day 775, and no information on the dust composition was available since the thermal emission was well fitted by a grey body (Wooden et al. 1993).

Taking the appearances of the blue-shifted lines, infrared excess and/or decline of optical luminosity as the diagnostics, so far dust formation in the ejecta has been reported in four SNe excluding SN 1987A (see the references in Table 1); three are Type II–P SNe which is the most common type among CCSNe (e.g. Smartt et al. 2009), and one is Type Ib. The evidence of dust formation in SN 2005af is based only on the mid-infrared (MIR) excess observed by Spitzer, but the detection of CO and SiO molecules supports the formation since CO and/or SiO molecules are detected prior to dust formation in Type II–P SNe. The molecules could play an important role in formation of dust because CO acts as a coolant in the ejecta (e.g. Liu & Dalgarno 1995), and SiO is considered to be a precursor of dust grains (Kozasa et al. 1989). The onset of dust formation ranges from  $\sim 300$  to  $\sim 600$  days after the explosion in Type II–P SNe. In SN 1990I, which is Type Ib, the onset seems to be earlier, as can be expected, because the escape of  $\gamma$ -rays with less effective deposition causes the gas in the ejecta to cool down faster without an H-envelope. The dust mass derived from the observations is less than  $10^{-3} M_{\odot}$ , although the observation of SN 1999em suggested that dust much more than  $10^{-4} M_{\odot}$  was produced in the ejecta (Elmhamdi et al. 2003).

Recently formation of dust in cool dense shells (CDSs) generated by the interaction of ejecta with a circumstellar medium (CSM) has been reported in three SNe summarized in Table 2 (see the references in Table 2); two are Type IIn and one is Type Ib, where the presence of dense circumstellar envelopes is confirmed by the X-ray observations (e.g. Smith et al. 2008a). The evidences come from the NIR/MIR excess and the concurrent appearance of the blueshift of the narrow lines in CSM and/or the intermediate-width components originating in shocked gas. Onset of dust formation depends on when the ejecta encounters with dense CSM. The early formation of dust at day  $\sim 50$  in SN 2006jc is consistent with the LBV-like outburst  $\sim 2$  yr prior to the explosion. The dust mass estimates are  $> 2 \times 10^{-3} M_{\odot}$  in SN 1998S, and  $3 \times 10^{-4}$  by day 230 in SN 2006jc, assuming carbon dust. It should be noted that in addition to the formation of dust in CDSs, we cannot deny the possibility that dust also forms in the expanding ejecta; see Smith et al. (2008b) for SN 2005ip; Sakon et al. (2009), Tominaga et al. (2008), and Nozawa et al. (2008) for SN 2006jc. Although the frequency of Type IIn SNe is rare among CCSNe (Gal-Yam et al. 2007; Smartt et al. 2009), these observations on dust formation in CDS provide a new window to investigate the formation process of dust in astrophysical environments.

Nowadays, based on the observations, the mass of dust formed in the ejecta has been claimed to be less than  $10^{-3} M_{\odot}$  and to be too small to contribute to the inventory of dust in our Galaxy. However, we should keep in mind that the conclusion is not necessarily definite, based on the limited number of the observations and the assumption that thermal radiation from dust is optically

Table 1. Formation of dust in the ejecta. References; 1) Lucy et al. (1991), 2) Meikle et al. (1993), 3) Roche et al. (1989), 4) Whitelock et al. (1989), 5) Suntzeff & Bouchet (1990), 6) Lucy et al. (1989), 7) Catchpole & Glass (1987), 8) Aitken et al. (1988), 9) Ercolano et al. (2007), 10) Elmhamdi et al. (2004), 11) Elmhamdi et al. (2003), 12) Spyromilio et al. (2001), 13) Sugeran et al. (2006), 14) Hendry et al. (2005), 15) Meikle et al. (2007), 16) Kotak (2008), 17) Kotak et al. (2006). Note; The optical depth of the dust core derived from [O I] line profile  $\tau_d \gg 10$  at day 510 in SN 1999em (Elmhamdi. et al. 2003), which is much larger than  $\tau_d \sim 1$  in SN 1987A (Lucy et al. 1991).

name	Type	onset of dust formation $t_c$ [day]	IR excess (NIR/MIR)	decline of opt. lum.	blue-shifted lines	molecules	$M_d$ [ $M_\odot$ ]
SN 1987A	II-pec.	$\sim 350$ – $530$ <sup>1),2)</sup>	MIR <sup>3)</sup>	yes <sup>4),5)</sup>	[Mg I],[O I] etc. <sup>6)</sup>	CO <sup>7)</sup> , SiO <sup>8)</sup>	$7.5 \times 10^{-4}$ <sup>9)</sup>
SN 1990I	Ib	$\sim 250$ <sup>10)</sup>	–	yes <sup>10)</sup>	[O I], [Ca II] <sup>10)</sup>	–	–
SN 1999em	II-P	$465 < t_c < 510$ <sup>11)</sup>	–	yes <sup>11)</sup>	[O I],[Mg I],etc. <sup>11)</sup>	CO <sup>12)</sup>	$\geq 10^{-4}$ <sup>11)</sup>
SN 2003gd	II-P	$250 < t_c < 493$ <sup>13)</sup>	MIR <sup>13)</sup>	yes <sup>13)</sup>	[O I], H $\alpha$ <sup>13),14)</sup>	CO,SiO ? <sup>15)</sup>	$4 \times 10^{-5}$ <sup>15)</sup>
SN 2005af	II-P	$214 < t_c < 571$ <sup>16)</sup>	MIR <sup>16)</sup>	–	–	CO,SiO <sup>17)</sup>	$\sim 4 \times 10^{-4}$ <sup>16)</sup>

Table 2. Formation of dust in a cool dense shell produced by the interaction with dense circumstellar medium. References; 1) Pozzo et al. (2004), 2) Gerardy et al. (2000), 3) Smith et al. (2008b), 4) Fox et al. (2009), 5) Smith et al. (2008a), 6) Mattila et al. (2008). Note: For SN 2005ip, Fox et al. (2009) suggested the early formation of dust at day  $\sim 50$ , but the spectroscopic observation (Smith et al.2008b) suggested the later formation. It should be noted that Smith et al. (2008b) have suggested formation of dust in the ejecta at earlier time.

name	Type	onset of dust formation $t_c$ [day]	IR excess (NIR/MIR)	decline of optical lum.	blue-shifted lines	molecules	$M_d$ [ $M_\odot$ ]
SN 1998S	IIn	$\sim 250$ <sup>1)</sup>	NIR <sup>1)</sup>	–	H $\alpha$ , He I <sup>1)</sup>	CO <sup>2)</sup>	$> 2 \times 10^{-3}$ <sup>1)</sup>
SN 2005ip	IIn	$\sim 730$ <sup>3)</sup>	NIR <sup>3,4)</sup>	–	He I <sup>3)</sup>	–	–
SN 2006jc	Ib	$\sim 50$ <sup>5,6)</sup>	NIR–MIR <sup>5,6)</sup>	yes	He I <sup>5,6)</sup>	–	$3 \times 10^{-4}$ <sup>6)</sup>

thin in some cases; as pointed out by Meikle et al. (2007), the dust may reside in optically thick clumps in the ejecta. Also, the NIR–MIR observations could miss the cool dust, since dust grains might cool down quickly after the formation as is demonstrated by Nozawa et al. (2008). Therefore, the monitorings of various types of SNe after the explosions, covering the temporal and wavelength ranges as wide as possible, are necessary to reveal the mass of dust formed in the ejecta and its dependence on the type of SNe. In addition the sophisticated radiative transfer calculations such as those carried out by Sugerman et al. (2006) and Ercolano et al. (2007) are inevitable to derive the dust mass from the observations relevant to dust formation, taking into account the more realistic spatial distribution and chemical composition of dust in the ejecta.

### 3. Formation of dust in the ejecta

In this section we investigate how the formation process of dust in the ejecta depends on the type of SNe, focusing on Type II–P and Type IIb SNe whose progenitors are evolved from massive stars with solar metallicity. The calculation of dust formation is based on the theory of nucleation and growth developed by Nozawa et al (2003), taking into account chemical reaction at the condensation by considering that the key species, defined as a gas species with the least collisional frequency among the reactants, controls the kinetics of nucleation and grain growth (Kozasa & Hasegawa 1987, Hasegawa & Kozasa 1988)<sup>1</sup>. Given the time evolution of gas density and temperature together with the elemental composition, we can determine when, where, what kind, what size, and how much mass of dust condenses in the ejecta.

#### 3.1. Models of supernovae and dust formation calculation

Formation process of dust grains in the ejecta of SNe is controlled by the time evolution of gas density and temperature as well as the elemental composition in the ejecta as demonstrated by Kozasa et al. (1989). Thus, we apply the hydrodynamic model of a SN explosion for the time evolution of the gas density and the nucleosynthesis calculation for the elemental composition in the ejecta. The time evolution of the gas temperature is calculated by solving the radiative transfer equation taking into account the energy deposition from radioactive elements. Table 3 summarizes the models of SNe used for the calculations.

In the calculations we consider that dust forms within the He–core because the large expansion velocity in the outer envelope causes the density of condensible elements to be too low to form dust grains. For the elemental composition, we do not consider any mixing since the mixing driven by the Rayleigh–Taylor instability in the ejecta at the explosion is not microscopic but macroscopic as have been revealed by the observation of Cas A (Douvion et al. 1999; Ennis et al. 2006). We assume that formation of CO and SiO molecules is complete; all carbon (silicon) atoms are locked into CO (SiO) molecules in the locations where C/O (Si/O) is less than 1. This implies that C–bearing dust condenses only in

---

<sup>1</sup>There was a typo in the nucleation rate  $J$  in Kozasa & Hasegawa (1987) and Nozawa et al. (2003); replace  $c_1$  with  $c_1^2$ , where  $c_1$  is the number density of key species.



Table 3. Models of SNe;  $M_{\text{pr}}$  is the progenitor mass,  $E_{\text{exp}}$  the kinetic energy of the explosion,  $M(^{56}\text{Ni})$  the mass of  $^{56}\text{Ni}$  in the ejecta,  $M_{\text{eje}}$  the mass of the ejecta,  $M_{\text{H-env}}$  the mass of the hydrogen envelope,  $M_{\text{He-core}}$  the mass of the He-core, and  $M_{\text{metal}}$  the mass of metal inside the He-core. Model A is taken from Nomoto et al. (2006), and model B from Umeda and Nomoto (2002).

model	Type	$M_{\text{pr}}$ [ $M_{\odot}$ ]	$E_{\text{exp}}$ [erg]	$M(^{56}\text{Ni})$ [ $M_{\odot}$ ]	$M_{\text{eje}}$ [ $M_{\odot}$ ]	$M_{\text{H-env}}$ [ $M_{\odot}$ ]	$M_{\text{He-core}}$ [ $M_{\odot}$ ]	$M_{\text{metal}}$ [ $M_{\odot}$ ]
A	II-P	15.0	$10^{51}$	0.134	12.2	10.4	1.80	0.482
B	II-P	20.0	$10^{51}$	0.07	15.7	10.9	4.77	3.35
C	I Ib	18.0	$10^{51}$	0.07	2.94	0.08	2.86	1.297

the region of  $\text{C}/\text{O} > 1$ ; see Todini & Ferrara (2001) and Bianchi & Schneider (2007) for the calculation of dust formation assuming the uniform mixing of elements and considering formation processes of CO and SiO in the ejecta.

Figure 1 shows the elemental composition within the He-core for a Type II-P SN (model A; upper panel) and for a Type I Ib SN (model C; lower panel). From the view point of dust formation, the He-core is roughly divided into four layers; the outer C-rich layer, the O-rich layer, the Si-S-Fe layer and the Fe-S-Si layer. What kind of dust grain really condenses depends on the details of elemental composition. Thus, in the calculation we simultaneously solve the equations of nucleation and grain growth for 19 possible condensates (see Nozawa et al. 2003 for details).

Figure 2 shows the time evolution of the gas density and temperature in the ejecta; Left panel for Type II-P SN (model A) and right panel for Type I Ib SN (model C). It should be noted that the gas density in the ejecta of Type I Ib SN is more than three orders of magnitude smaller than that of type II-P SN, because the expansion velocity in the ejecta is much higher in Type I Ib SN without thick H-envelope. The time evolution of the gas temperature depends on the model through the mass of H-envelope and  $M(^{56}\text{Ni})$  in the ejecta.

### 3.2. Results of dust formation calculations

Figure 3 shows the condensation time of each grain species formed in the ejecta; Left for Type II-P SN (model A) and right for Type I Ib SN (model C). As the gas in the ejecta cools down with time, C grains start to condense first in the C-rich layer around day 300 after the explosion. Afterwards, in the oxygen-rich layer,  $\text{Al}_2\text{O}_3$ ,  $\text{Mg}_2\text{SiO}_4$ ,  $\text{MgSiO}_3$  and  $\text{SiO}_2$  condense in this order from day 350 to day 450. In the Si-S-Fe rich layer, FeS and Si condense around day 450 in Type II-P SN and around day 630 in Type I Ib SN. After then, in the innermost Fe-S-Si layer, Si, FeS and Fe condense in Type II-P SN, but Si and FeS in Type I Ib SN. The condensation sequence of MgO and  $\text{Fe}_3\text{O}_4$  in the O-rich layer is different between Type II-P SN and Type I Ib SN, depending on the detailed density structure and elemental composition in the ejecta. Also small amount of FeS and Si condenses from 450 to 500 days in the C-rich layer of Type II-P SN, and so does FeS around day 580 in the O-rich layer of Type I Ib SN.

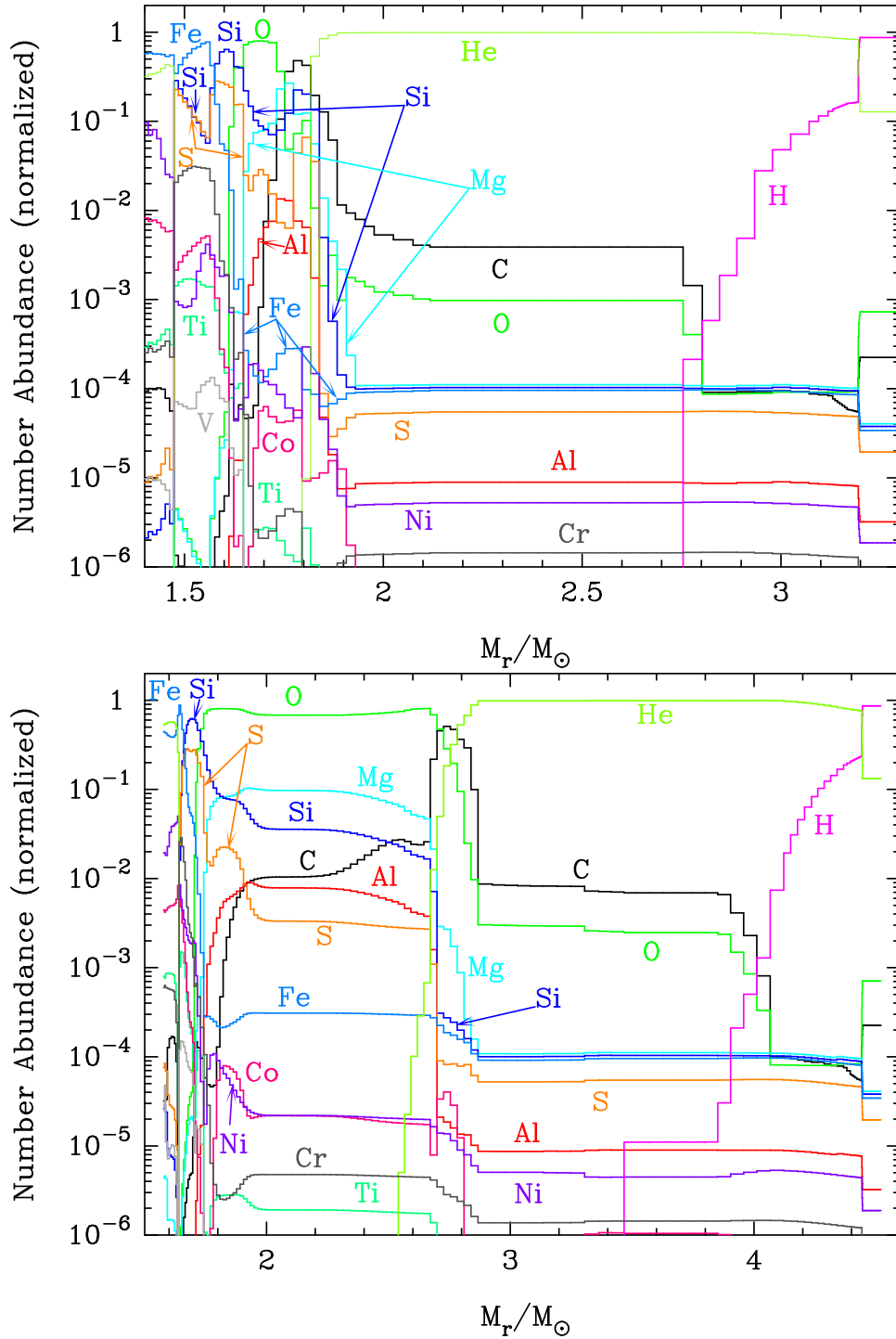


Figure 1. Elemental composition within He-core: Upper panel for Type II-P SN (model A) and lower panel for Type IIb SN (model C). Note that the position in the ejecta is indicated by the mass coordinate that is defined as the enclosed mass from the center.



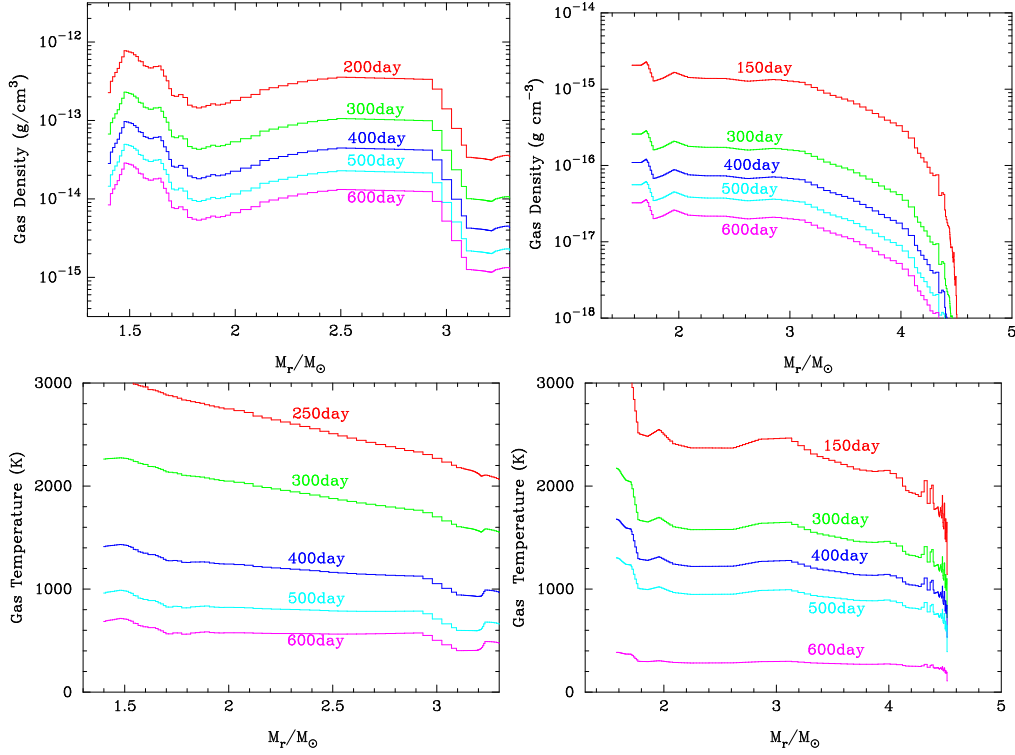


Figure 2. Time evolution of gas density and temperature in the ejecta; Left panel for Type II-P(model A) and right panel for Type IIb (model C)

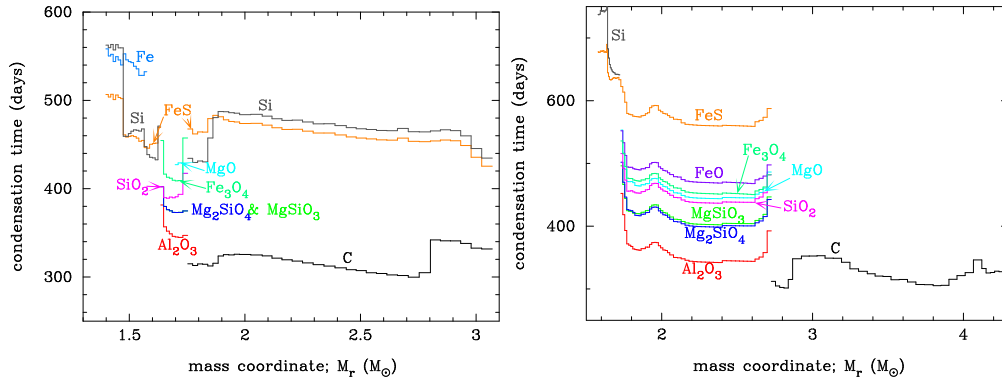


Figure 3. Condensation times of dust species formed in the ejecta; Left for Type II-P SN (model A) and right for Type IIb SN (model C). The condensation time is defined as the time at which the nucleation rate reaches the maximum. The condensation times of dust species in the C and O-rich layers are a little earlier in Type II-P than in Type IIb, except for FeS and Si in C-rich layer of Type II-P SN, and FeS in Type IIb

Figure 4 shows the average radius of each dust species formed in the ejecta. In Type IIb SN (right panel), the average radii of all grain species are smaller than  $0.01 \mu\text{m}$  due to the low gas density in the ejecta. On the other hand, the

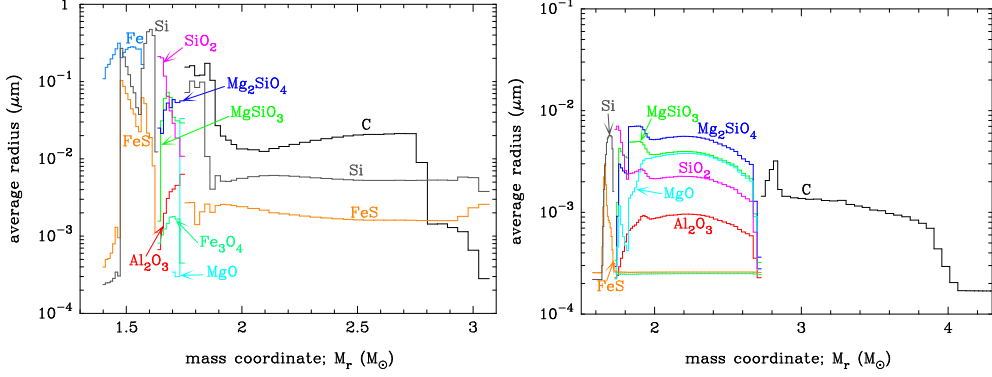


Figure 4. Average radii of dust species formed in the ejecta: Left for Type II-P SN (model A) and right for Type IIb SN (model C)

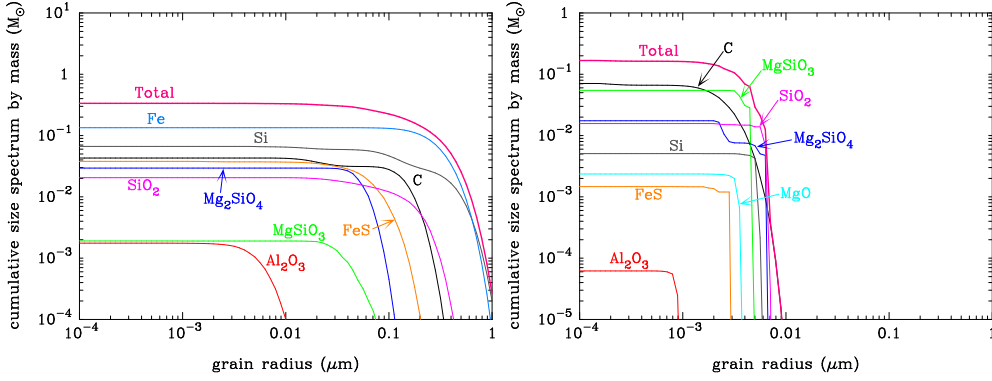


Figure 5. Cumulative size distributions of dust species by mass summed up over the ejecta. The mass is dominated by dust grains with radii larger than  $0.03 \mu\text{m}$  for Type II-P SN (model A; left), but with radii less than  $0.006 \mu\text{m}$  for Type IIb SN (model C; right)

average radii of dust grains are larger than  $0.01 \mu\text{m}$  in Type II-P (left panel), except for Si and FeS in the C-rich layer, and  $\text{Al}_2\text{O}_3$ , MgO and  $\text{Fe}_3\text{O}_4$  in the O-rich layer. The difference in the size of dust grains between Type II-P SN and Type IIb SN is much more clearly represented by the cumulative size distribution of dust by mass summed up over the ejecta, which is given in Figure 5. Except for  $\text{Al}_2\text{O}_3$ , the dust mass is dominated by grains with radii larger than  $0.03 \mu\text{m}$  in Type II-P SN (model A; left panel), while the dust mass of all species is dominated by the grains whose radii are less than  $0.006 \mu\text{m}$  in Type IIb (model C; right panel). This leads to the big difference in the fate of dust grains in SNRs as is presented in the next section.

Table 4 summarizes the mass of dust formed in the ejecta of Type II-P SNe (model A and B) and Type IIb SN (model C). The masses of C, Mg-silicates ( $\text{Mg}_2\text{SiO}_4$  and  $\text{MgSiO}_3$ ),  $\text{SiO}_2$ , Si and FeS do not depend so much on the model, while masses of  $\text{Al}_2\text{O}_3$ , MgO,  $\text{Fe}_3\text{O}_4$  and Fe are different from model to model, depending on the detailed elemental composition and density structure in the ejecta. Generally the total dust mass increases with increasing progenitor

Table 4. Dust mass formed in the the ejecta

model	A	B	C
Type	II-P	II-P	I Ib
$M_{\text{pr}}[M_{\odot}]$	15	20	18
dust species	$M_{\text{d},j}[M_{\odot}]$		
C	$4.30 \times 10^{-2}$	$4.00 \times 10^{-2}$	$7.08 \times 10^{-2}$
$\text{Al}_2\text{O}_3$	$1.76 \times 10^{-3}$	$4.33 \times 10^{-2}$	$6.19 \times 10^{-5}$
$\text{Mg}_2\text{SiO}_4$	$2.95 \times 10^{-2}$	0.133	$1.74 \times 10^{-2}$
$\text{MgSiO}_3$	$1.91 \times 10^{-3}$	$5.68 \times 10^{-3}$	$5.46 \times 10^{-2}$
MgO	$3.19 \times 10^{-7}$	0.159	$2.36 \times 10^{-3}$
$\text{SiO}_2$	$2.06 \times 10^{-2}$	$8.21 \times 10^{-2}$	$1.57 \times 10^{-2}$
$\text{Fe}_3\text{O}_4$	$5.60 \times 10^{-5}$	$1.55 \times 10^{-3}$	
FeS	$3.79 \times 10^{-2}$	$5.66 \times 10^{-2}$	$1.47 \times 10^{-3}$
Si	$6.65 \times 10^{-2}$	$9.04 \times 10^{-2}$	$5.07 \times 10^{-3}$
Fe	0.134	$6.46 \times 10^{-2}$	
total mass	0.327	0.676	0.167
$M_{\text{d}}/M_{\text{metal}}$	0.695	0.202	0.129

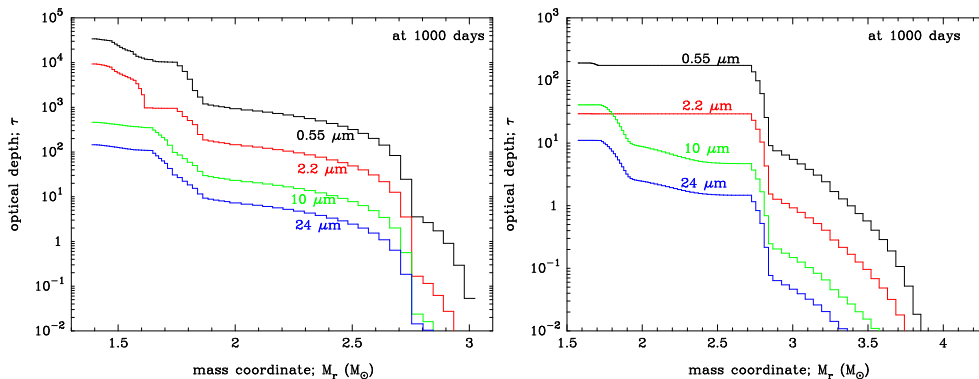


Figure 6. Optical depth of the ejecta at 1000 days after explosion as a function of mass coordinate; Left for Type II-P SN (model A) and right for Type I Ib SN (model C).

mass. The total dust mass  $M_{\text{d}}$  ranging from  $\sim 0.17$  to  $0.68 M_{\odot}$  is two to three orders of magnitude larger than the mass inferred from the observations. The condensation efficiencies defined by  $M_{\text{d}}/M_{\text{metal}}$  ranges from 0.13 (model C) to 0.7 (model A). The condensation efficiency of model A is significantly higher than in the other models, because the metal mass within the He-core is smaller due to the thin O-rich layer (see Table 1 and Figure 1). Thus, being different from the total dust mass, the condensation efficiency strongly depends on the detailed density structure and elemental composition in the ejecta.

Finally we present the optical depth of the ejecta at day 1000 after the explosion in Figure 6. The optical depth of the ejecta after dust formation decreases proportional to  $t^{-2}$  since the ejecta expands homologously. Thus, around day 500 after the onset of dust formation, the ejecta is optically thick

even at  $24 \mu\text{m}$  except for the outer  $\sim 0.3 M_{\odot}$  ( $1.5 M_{\odot}$ ) region for model A (model C). This result suggests that it could be inappropriate to estimate dust mass from the thermal emission by assuming the ejecta to be optically thin at MIR. It takes about 800 (60) yr at  $0.5 \mu\text{m}$  for the entire ejecta to be optically thin, and about 50 (10) yr at  $24 \mu\text{m}$  for model A (model C).

#### 4. Evolution of dust in supernova remnant

Dust grains formed in the ejecta suffer from erosion and destruction by sputtering in the hot gas between the reverse and forward shocks produced by the interaction of the ejecta with the surrounding medium. This process determines how much mass and what kind of dust can survive and be injected into ISM. In this section we demonstrate the evolution of dust in SNRs, focusing on type IIb SN (model C). Then, we calculate the time evolution of thermal emission from dust in the SNR and compare with the observation of Cas A.

##### 4.1. Motion and destruction of dust in SNRs

At the time when the ejecta encounters the ISM surrounding the SN, the forward shock propagating into the ISM and the reverse shock into the ejecta are generated (e.g. Truelove and McKee 1999), and the gas swept up by the shocks is heated up and ionized. The dust grains hit by the reverse shock are injected into the shocked gas with a velocity relative to the gas; gas is decelerated by the shock, while dust grains decoupling from gas penetrate into the hot gas with the same velocity just before the encounter. Then dust grains are decelerated and eroded by collision with gas. The deceleration of dust by the gas drag is inversely proportional to  $\rho_d a$ , and the erosion rate of dust by sputtering is almost independent of  $a$  (e.g. Dwek & Arendt 1992), where  $a$  and  $\rho_d$  is the radius and the bulk density of dust, respectively. As a result, the small sized/low density dust is easily trapped into gas, and is eroded by non-kinetic (thermal) sputtering, while larger sized/high density dust moves through the gas, suffering kinetic sputtering.

We calculate the motion and destruction of dust in the SNR, adapting the model for the SN explosion as the initial conditions for gas velocity and density, and applying the results of dust formation calculations as the initial spatial and size distributions of dust grains in the ejecta. The method of calculation and the underlying assumptions are the same as those by Nozawa et al. (2007). In the calculations, we assume that the ejecta expands into a uniform medium with solar metallicity. We consider the two cases for the ambient hydrogen number density;  $n_{\text{H}} = 1.0$  and  $10.0 \text{ cm}^{-3}$ . We assume the gas temperature in the ambient medium  $T_{\text{g,amb}} = 10^4 \text{ K}$ , and that the ejecta hits the ISM at  $t_{\text{enc}} = 10 \text{ yr}$  after the explosion. Note that the assumptions on  $T_{\text{g,amb}}$  and  $t_{\text{enc}}$  do not significantly affect the result of calculations. The sputtering yield of each grain species is taken from Nozawa et al. (2006).

The left panel of Figure 7 shows the time evolution of gas density and temperature in the SNR of type IIb SN (Type IIb SNR) for  $n_{\text{H}} = 10 \text{ cm}^{-3}$ ; the positions of the reverse (forward) shock at given times are indicated by upward (downward) arrows. The temperature of gas hit by the shocks quickly rises up to  $10^7$  to  $10^9 \text{ K}$ , and is kept to be  $> 10^5 \text{ K}$  until the cool dense shell forms behind

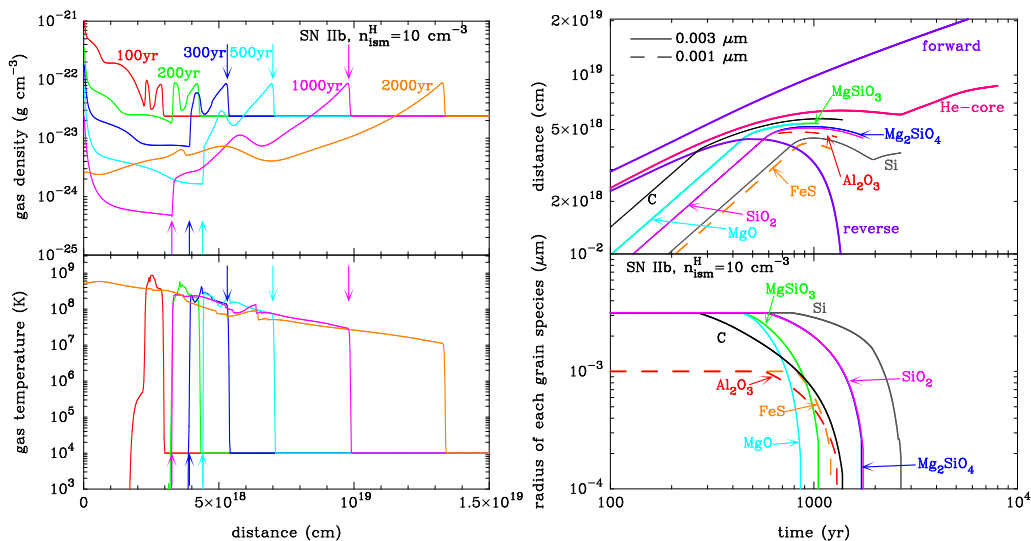


Figure 7. Time evolution of gas density and temperature (left panel), and the motion and destruction of dust grains (right panel) in the Type IIb SNR for  $n_{\text{H}} = 10.0 \text{ cm}^{-3}$

the forward shock at  $t \sim 10^6$  yr after the explosion. The reverse shock encounters the C-rich layer at  $\sim 80$  yr, the O-rich layer at  $\sim 440$  yr, the Si-S-Fe rich layer at  $\sim 800$  yr, and the Fe-Si-S rich layer at  $\sim 880$  yr after the explosion, and the ejecta are completely swept up by the reverse shock in  $\sim 1400$  yr. The right-upper panel shows the trajectories of dust species with radii of  $0.001 \mu\text{m}$  (dashed curves) and  $0.003 \mu\text{m}$  (solid curves) together with the positions of the forward and reverse shocks and the outer boundary of He-core. The time evolution of the radius of each grain species is depicted in the right-lower panel. As can be seen, grains with radii of  $0.003 \mu\text{m}$  are quickly trapped into the hot gas behind the reverse shocks and are completely destroyed by thermal sputtering within  $\sim 3 \times 10^3$  yr. How long dust grains remain in SNR depends not only on the initial position but also on the chemical composition.

The time evolution of the mass of each dust species in the hot gas of Type IIb SNR is displayed in Figure 8; Left for  $n_{\text{H}} = 1.0 \text{ cm}^{-3}$ , and right for  $n_{\text{H}} = 10.0 \text{ cm}^{-3}$ . Except for C grains for  $n_{\text{H}} = 1.0 \text{ cm}^{-3}$ , all dust grains are destroyed in  $t < 3 \times 10^4$  ( $4 \times 10^3$ ) yr for  $n_{\text{H}} = 1.0$  ( $10.0$ )  $\text{cm}^{-3}$ . Although the time necessary for the reverse shock to reach the dust forming layer is almost two times longer for  $n_{\text{H}} = 1.0 \text{ cm}^{-3}$  than for  $n_{\text{H}} = 10.0 \text{ cm}^{-3}$ , it takes much longer for dust grains to be destroyed for  $n_{\text{H}} = 1.0 \text{ cm}^{-3}$  because the lower density in the hot gas caused by the delayed encounter reduces the erosion rate of dust by sputtering significantly. It should be noted that C grains dominate the dust mass almost over all times for  $n_{\text{H}} = 1.0 \text{ cm}^{-3}$ , while for  $n_{\text{H}} = 10.0 \text{ cm}^{-3}$  the mass of C grains quickly decreases at  $t > 300$  yr, and then  $\text{MgSiO}_3$  and  $\text{SiO}_2$  grains dominate the dust mass in the SNR. Thus, the ambient gas density strongly affects not only the mass but also the composition of dust grains remaining in the SNR.

Table 5 presents the surviving dust mass  $M_{\text{surv}}$  at  $t = 10^5$  yr for the models. Although  $M_{\text{surv}}$  decreases with increasing  $n_{\text{H}}$ , how much mass of dust survives

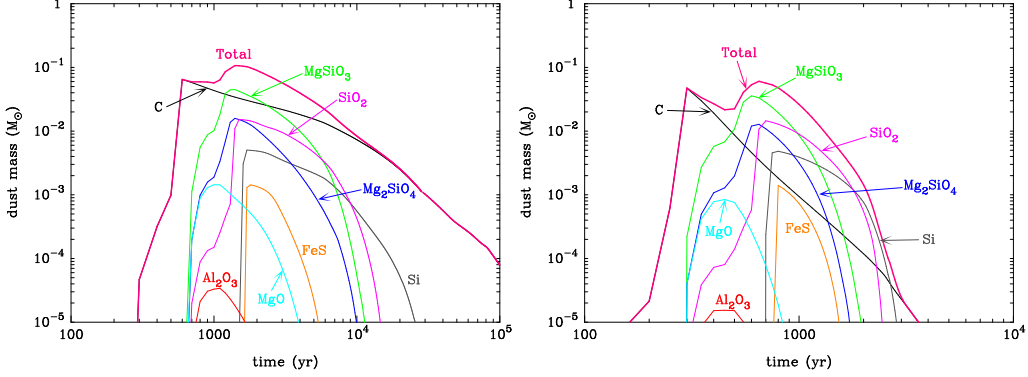


Figure 8. Time evolution of dust mass in the shocked gas of the Type IIb SNR: Left for  $n_{\text{H}} = 1.0 \text{ cm}^{-3}$  and right for  $n_{\text{H}} = 10.0 \text{ cm}^{-3}$ .

Table 5. Mass of dust surviving in the SNRs  $M_{\text{surv}}$  at  $t=10^5 \text{ yr}$  and the efficiency of survival defined by  $\eta = M_{\text{surv}}/M_{\text{d}}$

$n_{\text{H}}[\text{cm}^{-3}]$	1.0		10.0	
model (type)	$M_{\text{surv}}[M_{\odot}]$	$\eta$	$M_{\text{surv}}[M_{\odot}]$	$\eta$
A (Type II–P)	0.190	0.581	0.104	0.318
B (Type II–P)	$5.66 \times 10^{-2}$	$8.37 \times 10^{-2}$	$3.91 \times 10^{-2}$	$5.78 \times 10^{-2}$
C (Type IIb)	$7.83 \times 10^{-5}$	$6.07 \times 10^{-4}$	0.00	0.00

strongly depends on the type of SNe through the thickness of outer H–envelope that influences the size of dust formed in the ejecta as well as the time when the reverse shock reaches the dust forming layers. In the Type IIb SNR, dust is destroyed quickly partly because the small sized dust grains with radii  $< 0.006 \mu\text{m}$  populate the remnant region. In addition, the earlier arrival of reverse shock at the dust–forming layer causes the gas density behind the reverse shock to be higher, and enhances the erosion rate of dust grains; for example, the 35 times earlier arrival to the C–rich layer compared to the Type II–P SNR (model A) results in the 10 times higher gas density behind the reverse shock in the Type IIb SNR. However, it should be noted that, contrary to the expectation, dust grains are more destroyed in model B than in model A, despite that the mass of H–envelope is almost same. One of the reasons is that MgO grains with a sputtering rate somewhat larger than others grains (Nozawa et al. 2006) are more abundant in model B (see Table 4), and another is that the sizes of Fe and Si grains in model A are significantly larger than those in model B. Thus, the survival of dust grains in SNR depends on not only the thickness of H–envelopes but also on the detailed chemical composition, size distribution, and the amount of dust grains formed in the ejecta.

The efficiency of survival  $\eta$  defined as  $M_{\text{surv}}/M_{\text{d}}$  is larger than  $\sim 0.06$  in the Type II–P SNR, but less than  $6 \times 10^{-4}$  in the Type IIb SNR. Dust grains surviving at  $t = 10^5 \text{ yr}$  are almost free from the destruction by sputtering, and

are trapped into the dense cool shell formed behind the forward shock or injected into the ISM. Thus, the injection efficiency strongly depends on the type, which should be incorporated into chemical evolution models of dust in the ISM. In addition, it should be mentioned here that the survival in SNRs and the injection into the ISM of newly formed dust depend on the density structure in the ISM as well as the inhomogeneity in the ejecta. For the ambient medium whose gas density decreases as  $r^{-n}$  with distance  $r$ , the time evolution of the density of gas swept up by the reverse shock is different from that for a constant density as shown by Chevalier & Oishi (2003), which affects the evolution of dust in SNRs. If dust grains reside in dense clumps (knots) as suggested by the observations (e.g. Arendt, Dwek, & Moseley 1999), the dust grains could survive, since the reverse shock encountering dense clumps could indeed be radiative so that the gas temperature could stay cool enough for dust grains to be rescued from the destruction by sputtering. These aspects should be explored to reveal how much mass of dust grain can survive in SNRs and be injected into the ISM.

#### 4.2. Thermal emission from dust in Type IIb SNR

Dust grains formed in the ejecta and injected into the hot plasma between the reverse and forward shocks are heated up by collision with gas, and emit thermal radiation. The equilibrium temperature of dust grain is determined by balancing the collisional heating with the radiative cooling. However, in a rarefied hot plasma such as in SNRs, small sized dust grains undergo stochastic heating which affects the emissivity and the resulting spectral energy distribution (SED); see Dwek (1986) and Dwek et al. (2008) for details.

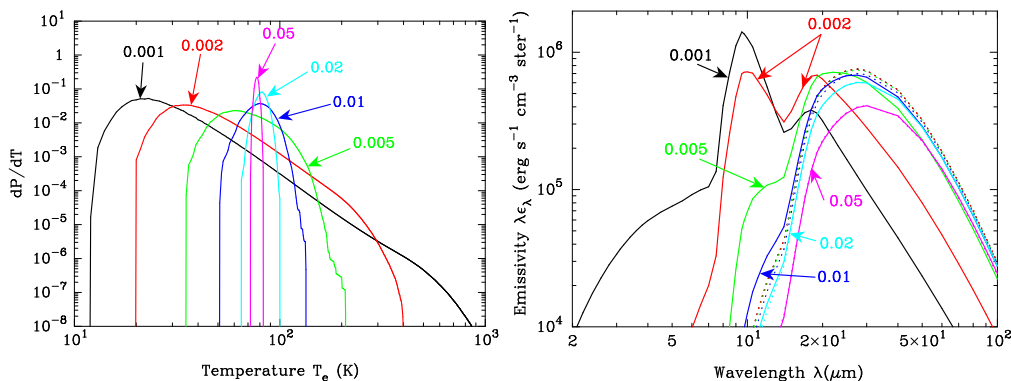


Figure 9. Temperature distribution functions of small astronomical silicate in the hot plasma with  $n_e = 10\text{cm}^{-3}$  and  $T_e = 10^7$  K (left) and the emissivities (right) for given radii, where the radius is in units of  $\mu\text{m}$ .

For example, Figure 9 shows the temperature distribution function and the emissivity of astronomical silicate (Draine and Lee 1984) embedded in a hot plasma with the electron temperature of  $T_e = 10^7$  K and number density of  $n_e = 10.0\text{ cm}^{-3}$ , which is calculated by a Monte-Carlo method. The fraction of incident energy that is deposited in a grain is calculated by fitting the experimental data of the stopping ranges of electrons tabulated by Iskef et al. (1983), according to the method by Dwek (1987b). With decreasing radius, the temperature distribution function becomes broader and the resulting emissivity



deviates strongly from the emissivity calculated by the equilibrium temperature; the deviation becomes significant for the radius of  $a < 0.02\mu\text{m}$ .

Taking into account the stochastic heating, we demonstrate the time evolution of thermal emission from dust grains embedded in the shocked gas in the Type IIb SNR, based on the results of dust formation and evolution calculations for Type IIb SN presented in § 3 and § 4.1. In the calculations, the heat capacities of grain species are taken from Takeuchi et al. (2005), and we use the same optical constants as those of Hirashita et al. (2005), except for amorphous  $\text{Al}_2\text{O}_3$  (Begemann et al. 1997 for the wavelength  $\lambda > 8\mu\text{m}$ ),  $\text{SiO}_2$  (Phillip 1985) and Si (Pillar 1985). We consider only collision with electrons for heating, because the radii of dust grains formed in the ejecta are so small that dust grains injected into the hot gas are quickly trapped and comove with the gas, and the heating is dominated by collision with electrons. In order to compare with the observations of Cas A, we put the SNR at the distance of 3.4 kpc. Figure 10 and 11 show the time evolution of SED ranging from 200 to 1800 yr after the explosion for  $n_{\text{H}}=1.0$  and  $10.0\text{ cm}^{-3}$ , respectively, where the solid (dotted) curve denotes the SED with (without) stochastic heating. The solid circles are the flux densities subtracting the synchrotron radiation from the observed ones tabulated by Hines et al. (2004).

The SEDs taking into account the stochastic heating is completely different from those with the equilibrium temperatures, especially in the wavelengths shorter than  $20\mu\text{m}$ . After the reverse shock encounters the C-rich layer at  $\sim 180$  (80) yr for  $n_{\text{H}}=1.0$  ( $10.0$ )  $\text{cm}^{-3}$ , the thermal emission from the stochastically heated C grains contribute to the SED until the reverse shock encounters the O-rich layer. In the case of  $n_{\text{H}} = 1.0\text{ cm}^{-3}$ , the thermal emission from C grains dominates the SED over the entire simulation period considered in the calculation, because the mass of dust in the SNR is almost dominated by C grains as can be seen from Figure 8. The emission features of MgO appearing at  $\lambda \sim 16\mu\text{m}$  from  $t = 800$  to 1200 yr, Mg-silicates at  $\lambda \sim 10\mu\text{m}$  after  $t = 1200$  yr and  $\text{SiO}_2$  at  $\lambda \sim 20\mu\text{m}$  after  $t = 1600$  yr are not prominent, being overwhelmed by thermal emission from C grains. On the other hand, in the case of  $n_{\text{H}} = 10.0\text{ cm}^{-3}$ , with C grains being more efficiently destroyed by sputtering, the emission features from other dust grains get prominent with time, after the reverse shock encounters the O-rich layer at  $t \sim 400$  yr; although the feature of MgO is weak, the emission feature of Mg-silicates around  $10\mu\text{m}$  becomes noticeable at  $t = 600$  yr, after then the  $20\mu\text{m}$  feature of  $\text{SiO}_2$  is prominent at  $t = 800$  yr. With increasing time, the SED is dominated by the emission features from stochastically heated dust grains.

The result of calculations clearly demonstrates that the time evolution of the SED is very sensitive to the evolution of dust in SNRs through the destruction by sputtering and the stochastic heating, which strongly depends on the density in the ambient medium. It should be noted that the calculated SED cannot be reproduced by a single dust component with multiple temperatures.

### 4.3. Comparison with the observation of Cas A

Cas A is the nearby Galactic SNR well-studied at various wavelengths and was recently identified as Type IIb SN from the spectrum of the scattered light echo (Krause et al. 2008). The presence of dust formed in the ejecta has been

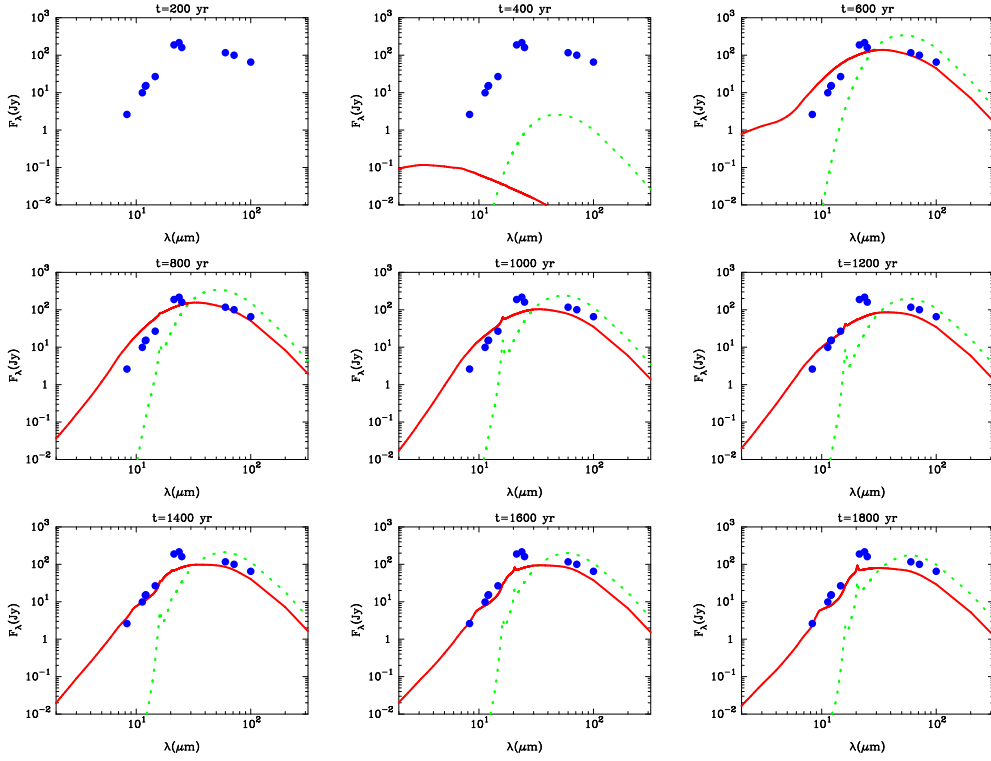


Figure 10. The time evolution of SEDs of Type IIb SNR for  $n_H = 1.0 \text{ cm}^{-3}$  with (solid curve) and without (dotted curves) stochastic heating. Closed circles are the flux densities subtracting the synchrotron radiation from the observed ones of Cas A (Hines et al. 2004)

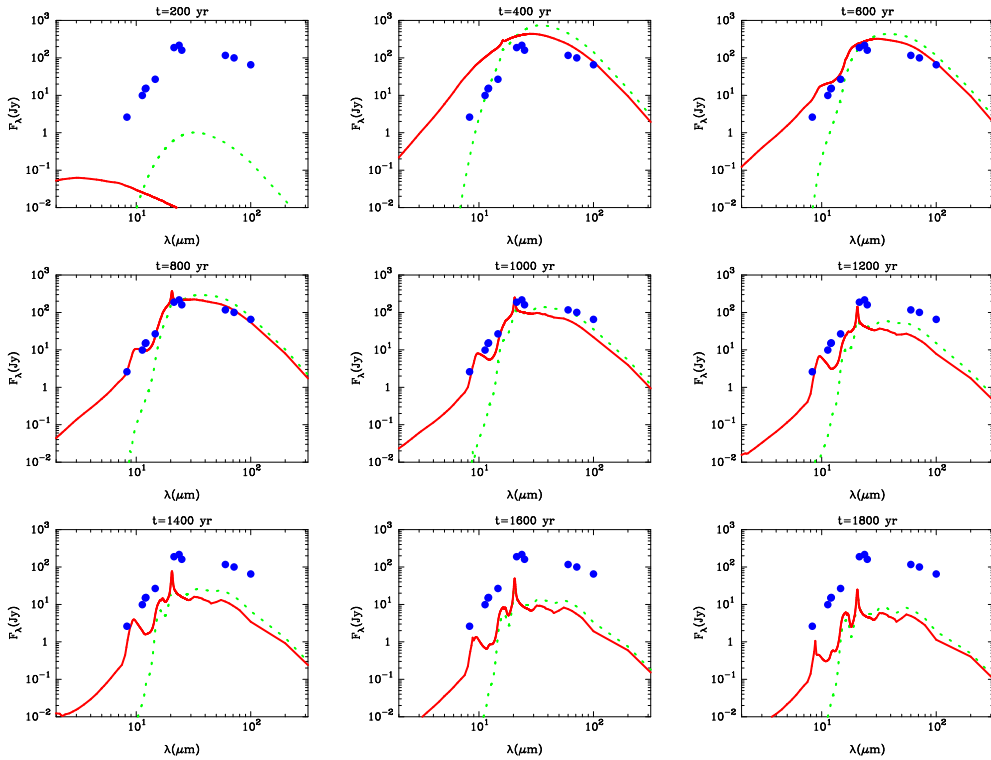


Figure 11. The same as Figure 10, but for  $n_H = 10.0 \text{ cm}^{-3}$

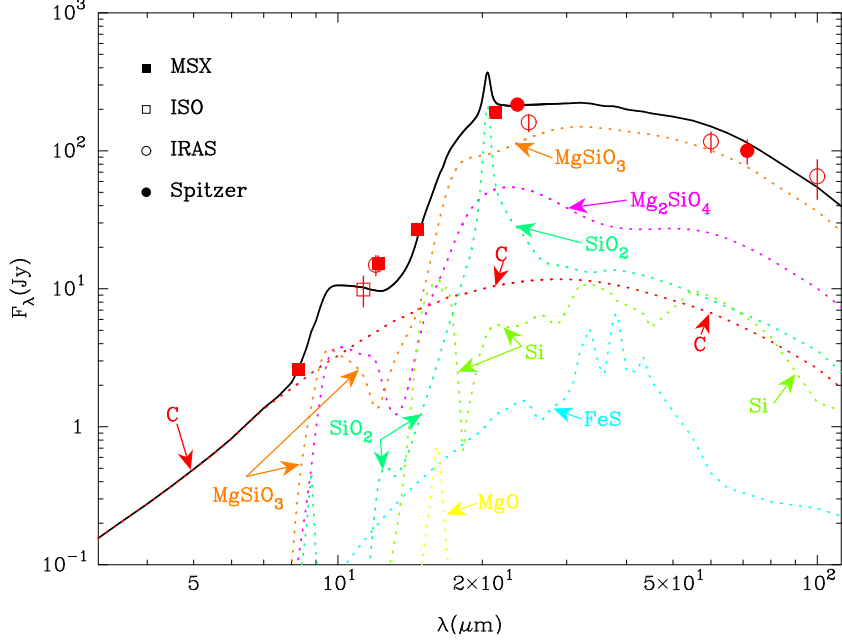


Figure 12. Comparison with the observation of Cas A. The symbols denote the flux densities of Cas A. The solid curve is the total flux density, and the dotted curves denote the contributions of each grain species.

confirmed by the infrared and submillimeter observations (Lagage et al. 1996; Arendt et al. 1999; Dunne et al. 2003). However, the dust mass derived from the observations has been controversial, ranging from  $< 1 \times 10^{-3}$  to  $\sim 1.0 M_{\odot}$  (Dwek et al. 1987a; Douvion, Lagage, & Pantin 2001; Dunne et al. 2003; Hines et al. 2004; Rho et al. 2008). The comparison of the calculated SED with the observations of Cas A could provide some insights on dust and its evolution in the Cas A SNR, although the models of Type IIb SN and the evolution of the SNR are not necessarily applicable to the Cas A SNR.

As shown in Figures 10 and 11, the calculated SEDs for  $n = 1.0 \text{ cm}^{-3}$ , being dominated by thermal emission from small C grains, cannot reproduce the observations at the wavelengths  $\lambda < 20 \mu\text{m}$  at  $t \leq 1000 \text{ yr}$ , and are significantly smaller than the observed flux densities at  $\lambda \geq 20 \mu\text{m}$ . On the other hand, for  $n_{\text{H}} = 10.0 \text{ cm}^{-3}$ , the calculated SED at  $t = 800$  around which the reverse shock encounters the Si-rich layer seems to reproduce the observed SED.

Figure 12 shows the detailed comparison of the SED calculated at  $t = 800$  yr with the observation and the contribution of each dust grains. Although the discrepancy around  $\lambda \sim 12 \mu\text{m}$  is remarkable and the  $20 \mu\text{m}$  feature of  $\text{SiO}_2$  is too sharp, the calculated SED can reasonably reproduce the overall shape of the observed SED without any tuning. The SED is dominated by Mg-silicates and  $\text{SiO}_2$  at  $\lambda > 15 \mu\text{m}$ , and by C and Mg-silicates at  $\lambda < 10 \mu\text{m}$ . The dominant dust species (the mass in unit of solar mass) are  $\text{MgSiO}_3$  ( $1.72 \times 10^{-2}$ ),  $\text{SiO}_2$  ( $1.08 \times 10^{-2}$ ),  $\text{MgSiO}_4$  ( $6.46 \times 10^{-3}$ ), Si ( $3.62 \times 10^{-3}$ ), C ( $1.6 \times 10^{-3}$ ), and FeS ( $1.04 \times 10^{-3}$ ). The total dust mass is  $\sim 0.04 M_{\odot}$ , which is consistent with the dust mass of  $0.02\text{--}0.054 M_{\odot}$  evaluated by Rho et al. (2008), apart from

the details. The presence of Si grains in the model indicates that the reverse shock already reaches a part of the inner Si–S–Fe layer, which is also not in contradiction with the observation of Cas A by Spitzer showing that the deeper Si–rich layer has been hit by the reverse shock in the region associated with the jet arising from the asymmetric explosion (Ennis et al. 2006).

## 5. Summary and concluding remarks

We calculate dust formation in the ejecta and evolution in the SNRs of Type II–P and IIb SNe in order to clarify how these processes depend on the type of CCSNe through the difference in the thickness (mass) of the outer envelope. We show that the mass of newly formed dust ranging from  $\sim 0.1$  to  $0.7 M_{\odot}$  does not so much depend on, but the size of dust grains is sensitive to the thickness of H–envelope. The radii of dust grains are less than  $0.006 \mu\text{m}$  in Type IIb SN with  $M_{\text{H–env}} = 0.08 M_{\odot}$ , while the dust mass is dominated by the grains with radii larger than  $0.03 \mu\text{m}$  in Type II–P SNe with  $M_{\text{H–env}} \sim 10 M_{\odot}$ . The difference in the size of the dust formed in the ejecta plays a crucial role in the evolution of dust in SNRs because the smaller sized grains are quickly trapped into the hot gas behind the reverse shock and are destroyed by sputtering. The surviving dust mass ranges from  $0.19$  to  $3.9 \times 10^{-2} M_{\odot}$  in the SNR of Type II–P SN for the ambient H number density of  $n_{\text{H}} = 1.0\text{--}10.0 \text{ cm}^{-3}$ , but the dust grains are almost completely destroyed in the SNR of Type IIb SN.

The SED of the thermal emission from dust embedded in SNRs can be applied as a diagnosis of the evolution of dust, reflecting the destruction by sputtering and the stochastic heating. The comparison of the calculated SED of Type IIb SNRs with the observation of Cas A suggests that the mass of dust in the SNR is  $0.04 M_{\odot}$ , which implies that the mass of dust formed in the ejecta is not less than  $1.0 \times 10^{-3} M_{\odot}$ , being different from the dust mass estimated from the dust forming CCSNe. In addition, Mg–silicates and  $\text{SiO}_2$  with mass reaching up to  $3.0 \times 10^{-2} M_{\odot}$  dominate the SED at  $\lambda > 15 \mu\text{m}$ , in contrast to the observed dust forming SNe that so far show no signature of silicates. This may indicate that these dust grains formed in the O–rich layer cool down quickly and evade being detected by the observations as is discussed by Nozawa et al. (2008).

It has been claimed that the mass of dust formed per CCSN is less than  $1.0 \times 10^{-3} M_{\odot}$  and is too small to contribute to the inventory of dust in ISM, based on the observations. However, it should bear in mind that the conclusion comes from a small number of observations. In order to clarify when how much mass and what kind of dust condenses in the ejecta of various types of SNe, it is inevitable to monitor SNe with temporal and wavelength coverages as wide as possible. In addition, the dedicated radiation transfer calculations such as those by Sugerman et al. (2006) and Ercolano et al (2007) are promising in evaluating the dust mass compared with the observations, taking into account the distribution and chemical composition of dust grains in the ejecta.

**Acknowledgments.** This work is partly supported by the Grant–in–Aid for Scientific Research of the Japan Society for the Promotion of Science (18104003, 20340038).

## References

- Aitken, D. K., Smith, C. H., James, S. D., Roche, P. F., Hyland, A. R., & MaGregor, P. J. 1988, *MNRAS*, 231, 7p
- Arendt, R. G., Dwek, E., & Moseley, S. H. 1999, *ApJ*, 521, 234
- Begemann, B., Dorschner, J., Henning, Th., Mutschke, H., Gürtler, J., Kömpe, C., & Nass, R. 1997, *ApJ*, 476, 199
- Bertoldi, F., Carilli, C. L., Cox, P., Fan, X., Strauss, M. A., Beelen, A., Omont, A., & Zylka, R. 2003, *A&A*, 406, L55
- Bianchi, S., & Schneider, R. 2007, *MNRAS*, 378, 973
- Catchpole, R., & Glass, I. 1987, *IAU Circ. No.* 4457
- Cernuschi, F., Marsicano, F., & Codina, S. 1967, *Annales d’Astrophysique*, 30, 1039
- Chevalier, R. A., & Oishi, J. 2003, *ApJ*, 593, L23
- Clayton, D. D., & Nittler, L. R. 2004, *ARA&A*, 42, 39
- Douvion, T., Lagage, P. O., & Cesarsky, C. J. 1999, *A&A*, 352, L111
- Douvion, T., Lagage, P. O., & Pantin, E. 2001, *A&A*, 369, 589
- Draine, B. T., & Lee, H. M. 1984, *ApJ*, 285, 89
- Dunne, L., Eales, S., Ivison, R., Morgan, H., & Edmunds, M. 2003, *Nat*, 424, 285
- Dwek, E. 1986, *ApJ*, 302, 363
- Dwek, E., Hauser, M. G., Dinnerstein, H. L., Gillett, F. C., & Rice, W. L. 1987a, *ApJ*, 315, 571
- Dwek, E. 1987b, *ApJ*, 322, 812
- Dwek, E., & Arendt, R. G. 1992, *ARA&A*, 30, 11
- Dwek, E. et al. 2008, *ApJ*, 676, 1029
- Elmhamdi, A., Danziger, I. J., Chugai, N., Pastorello, A., Turatto, M., Cappellaro, E., Altavilla, G., Benetti, S., Patat, F., & Salvo, M. 2003, *MNRAS*, 338, 939
- Elmhamdi, A., Danziger, I. J., Cappellaro, E., Della, V. M., Gouiffes, C., Phillips, M. M., & Turatto, M. 2004, *A&A*, 426, 963
- Ennis, J. A., Rudnick, L., Reach, W. T., Smith, J. D., Rho, J., DeLaney, T., Gomez, H., & Kozasa, T. 2006, *ApJ*, 652, 376
- Ercolano, B., Barlow, M. J., & Sugerman, B. E. K. 2007, *MNRAS*, 375, 753
- Filippenko, A. V. 1997, *ARA&A*, 35, 309
- Fox, O. et al. 2009, *ApJ*, 691, 650
- Gal-Yam, A. et al. 2007, *ApJ*, 656, 372
- Gerardy, C. L., Fesen, R. A., Höflich, P., & Wheeler, J. C. 2000, *AJ*, 119, 2968
- Hasegawa, H., & Kozasa, T. 1988, *Prog. Theor. Phys. Suppl.*, 96, 107
- Heger, A., Fryer, C. L., Woosley, S. E., Langer, N., & Hartmann, D. H. 2003, *ApJ*, 591, 288
- Hendry, M. A. et al. 2005, *MNRAS*, 359, 906
- Hillebrandt, W., & Niemeyer, J. C. 2000, *ARA&A*, 38, 191
- Hines, D. C. et al. 2004, *ApJS*, 154, 290
- Hirashita, H., Nozawa, T., Kozasa, T., Ishii, T. T., & Takeuchi, T. T. 2005, *MNRAS*, 357, 1077
- Iskef, H., Cunningham, J. W., & Watt, D. 1983, *Phys. Med. Biol.*, 28, 535
- Kotak, R. et al. 2006, *ApJ*, 651, L117
- Kotak, R. 2008, *IAU Symp.* 250, 437
- Kozasa, T., & Hasegawa, H. 1987, *Prog. Theor. Phys.*, 77, 1402
- Kozasa, T., Hasegawa, H., & Nomoto, K. 1989, *ApJ*, 344, 325
- Kozasa, T., Hasegawa, H., & Nomoto, K. 1991, *A&A*, 249, 474
- Krause, O., Birkmann, S. M., Usuda, T., Hattori, T., Goto, M., Rieke, G. H., & Misselt, K. A. 2008, *Sci*, 320, 1195
- Lagage, P. O., Claret, A., Ballet, J., Boulanger, F., Cesarsky, C. J., Cesarsky, D., Fransson, C., & Pollack, A. 1996, *A&A*, 315, L273
- Leibundgut, B. 2008, *General Relativity and Gravitation*, 40, 221
- Liu, W., & Dalgarno, A. 1995, *ApJ*, 454, 472

- Lucy, L. B., Danziger, I. J., Gouiffes, C., & Bouchet, P. 1989, in *Structure and Dynamics of Interstellar Medium*, IAU Colloq. No. 120, eds. G. Tenorio-Tagle et al. (New York: Springer), 164
- Lucy, L. B., Danziger, I. J., Gouiffes, C., & Bouchet, P. 1991, in *Supernovae*, ed. S. E. Woosley (New York: Springer), 82
- McCray, R. 1993, *ARA&A*, 31, 175
- Mattila, S. et al. 2008, *MNRAS*, 389, 141
- Meikle, W. P. S., Spyromilio, J., Allen, D. A., Varani, G.-F., & Cumming, R. J. 1993, *MNRAS*, 261, 535
- Meikle, W. P. S. et al. 2007, *ApJ*, 665, 608
- Nomoto, K., Tominaga, N., Umeda, H., Kobayashi, C., & Maeda, K. 2006, *Nuclear Physics A*, 777, 424
- Nozawa, T., Kozasa, T., Umeda, H., Maeda, K., & Nomoto, K. 2003, *ApJ*, 598, 785
- Nozawa, T., Kozasa, T., & Habe, A. 2006, *ApJ*, 648, 435
- Nozawa, T., Kozasa, T., Habe, A., Dwek, K., Umeda, H., Tominaga, N., Maeda, K., & Nomoto, K. 2007, *ApJ*, 666, 955
- Nozawa, T. et al. 2008, *ApJ*, 684, 1343
- Phillip, H. 1985, in *Handbook of Optical Constants of Solids*, ed. E. D. Palik, (San Diego: Academic Press), 749
- Piller, H. 1985, in *Handbook of Optical Constants of Solids*, ed. E. D. Palik, (San Diego: Academic Press), 571
- Pozzo, M., Meikle, W. P. S., Fassia, A., Geballe, T., Lundqvist, P., Chugai, N. N., & Sollerman, J. 2004, *MNRAS*, 352, 457
- Rho, J., Kozasa, T., Reach, W. T., Smith, J. D., Rudnick, L., Delaney, T., Eniss, J. A., Gomez, H., & Tappe, A. 2008, *ApJ*, 673, 271
- Roche, P. F., Aitken, D. K., Smith, C. H., & James, S. D. 1989, *Nat*, 337, 533
- Roche, P. F., Aitken, D. K., & Smith, C. H. 1991, *MNRAS*, 252, 39p
- Sakon, I. et al. 2009, *ApJ*, 692, 546
- Smartt, S. J., Eldridge, J. J., Crockett, R. M., Maund, J. R. 2009, *MNRAS*, in press
- Smith, N., Foley, R. J., & Filippenko, A. V. 2008a, *ApJ*, 680, 568
- Smith, N. et al. 2008b, arXiv:0809.5079
- Spyromilio, J., Leibundgut, B., & Gilmozzi, R. 2001, *A&A*, 376, 188
- Sugerman, B. E. K. et al. 2006, *Sci*, 313, 196
- Suntzeff, N. B., & Bouchet P. 1990, *AJ*, 99, 650
- Takeuchi, T. T., Ishii, T. T., Nozawa, T., Kozasa, T., & Hirashita, H. 2005, *MNRAS*, 362, 592
- Tominaga, N. et al. 2008, *ApJ*, 687, 1208
- Todini, P., & Ferrara, A. 2001, *MNRAS*, 325, 726
- Truelove, J. K., & McKee, C. 1999, *ApJS*, 120, 299
- Umeda, H., & Nomoto, K. 2002, *ApJ*, 565, 385
- West, R. M., Lauberts, A., Schuster, H. -E., & Jorgensen, H. E. 1987, *A&A*, 177, L1
- Wheeler, J. C., & Harkness, R. P. 1990, *Rep. Prog. Phys.*, 53, 1467
- Whitelock, P. A. et al. 1989, *MNRAS*, 240, 7p
- Wooden, D. H., Rank, D. M., Bregman, J. D., Witteborn, F. C., Tielens, A. G. G. M., Cohen, M., Pinto, P. A., & Axelrod, T. S. 1993, *ApJS*, 88, 477
- Wooden, D. H. 1997, in *Astrophysical Implications of the Laboratory Study of Presolar Materials*, AIP Conf. Ser. 402, eds. T. J. Bernatowicz & E. Zinner (New York, AIP), 317